

Magnetic Order-Disorder Transitions on a 1/3 - Depleted Square Lattice

H.-M. Guo^{1,3}, T. Mendes-Santos^{2,3}, W.E. Pickett³, and R.T. Scalettar³

¹*Department of Physics, Beihang University, Beijing, China*

²*Instituto de Física, Universidade Federal do Rio de Janeiro Cx.P. 68.528, 21941-972 Rio de Janeiro RJ, Brazil and*

³*Physics Department, University of California, Davis, California 95616, USA*

Quantum Monte Carlo simulations are used to study the magnetic and transport properties of the Hubbard Model, and its strong coupling Heisenberg limit, on a one-third depleted square lattice. This is the geometry occupied, after charge ordering, by the spin- $\frac{1}{2}$ Ni^{1+} atoms in a single layer of the nickelate materials $\text{La}_4\text{Ni}_3\text{O}_8$ and (predicted) $\text{La}_3\text{Ni}_2\text{O}_6$. Our model is also a description of strained graphene, where a honeycomb lattice has bond strengths which are inequivalent. For the Heisenberg case, we determine the location of the quantum critical point (QCP) where there is an onset of long range antiferromagnetic order (LRAFO), and the magnitude of the order parameter, and then compare with results of spin wave theory. An ordered phase also exists when electrons are itinerant. In this case, the growth in the antiferromagnetic structure factor coincides with the transition from band insulator to metal in the absence of interactions.

PACS numbers: 71.10.Fd, 75.47.Lx,

I. INTRODUCTION:

Over the last several decades, quantum Monte Carlo (QMC) methods have been widely used to investigate magnetic, charge, and pairing correlations in the Hubbard Hamiltonian on a square lattice¹⁻⁷. A central issue has been the intimate interplay between these different types of order, most fundamentally the possibility that magnetic correlations give rise to d -wave superconductivity. The occurrence of inhomogeneous (stripe) charge distributions upon doping the half-filled lattice, where antiferromagnetism (AF) survives in regions of low hole concentration but is suppressed on stripes of high concentration, has also been shown to have profound implications for pairing⁸.

In more recent studies, the effect of depletion of the square lattice has also been investigated. In this case, a regular removal of sites can be regarded as an extreme limit of the spontaneous formation of charge and spin patterns in which the degrees of freedom on certain sites are completely eliminated. Further types of transitions were then shown to occur within these geometries. Two prominent examples are the Lieb lattice⁹, where 1/4 of the sites are removed, giving rise to a flat electronic band and ferromagnetism, and the 1/5 depleted lattice¹⁰⁻¹⁴ where spin liquid phases compete with magnetic order. This latter geometry is realized by the vanadium atom locations in CaV_4O_9 , and also by some members of the iron-pnictide family^{15,16}. A crucial feature of this situation is the occurrence of two separate types of bonds, and hence of exchange or hopping energies, in the depleted structure.

Depleted lattices can also be formed starting from other, non-square, lattices. For example, the Kagomé lattice arises from removing one fourth of the sites of a triangular lattice. Like the Lieb lattice, the Kagomé structure has a flat band. However, because it is not bipartite, the band does not lie between the dispersing ones.

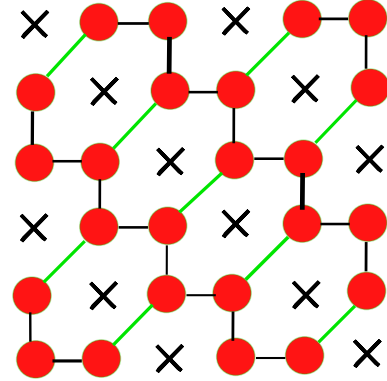


FIG. 1. The one third depleted square lattice. A regular diagonal stripe array of black crosses is removed, leaving the red site structure. We will assume two types of bonds exist corresponding to connections between NN (black) and NNN (green) sites of the original square geometry. (See text.)

In this paper, we investigate the magnetic and charge patterns within the 1/3 depleted square lattice of Fig. 1, which is formed by the red sites remaining after the removal of the black sites, which form stripes along one diagonal. The bonds between red sites are of two sorts: ones which were the near neighbor bonds of the original, full square lattice, and ones which connect through the diagonal rows of removed sites, and which were next near neighbors of the original lattice. This distinction will be modeled, in the following sections, by allowing for different energy scales on the two types of bonds. Notice that this lattice structure remains bipartite, a fact which has implications for AF order without frustration and also for the absence of a sign problem in QMC simulations.

Figure 1 is equivalent to a strained version of the honeycomb geometry realized in graphene. “Artificial graphene” lattices, can be achieved by nanopatterning¹⁷, by molecule-by-molecule assembly¹⁸, or by trapping

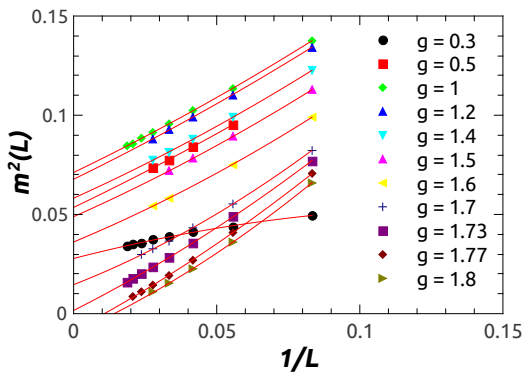


FIG. 2. Finite size scaling of the square of the AF order parameter m^2 for the spin-1/2 Heisenberg model. For a ratio $g > 1.75 = g_c$ of exchange couplings, a transition to a disordered spin liquid state occurs. LRAFO persists to small values of the interchain exchange. Data were obtained with the SSE algorithm.

ultracold atoms on optical lattices. They offer the possibility of tunable bond strengths, for example through application of strain, and have recently been discussed as a means for further investigation of Dirac particles and their associated correlated and topological phases¹⁹. Graphene with a “Kekulé distortion”^{18,20,21}, involves the appearance of two distinct bond hoppings, albeit in a pattern different from that of Fig. 1.

A second motivation for investigating the geometry of Fig. 1, which more directly connects with the notion of ‘depletion’ and which also fundamentally involves magnetic order, is provided by recent experimental²² and theoretical²³ studies of the layered nickelates $\text{La}_4\text{Ni}_3\text{O}_8$, and $\text{La}_3\text{Ni}_2\text{O}_6$. In these materials, the formal Ni valences of +1.33 and +1.5 are separated into charge ordered Ni^{1+} (spin $\frac{1}{2}$) and Ni^{2+} (spin 0), so that spin- $\frac{1}{2}$ stripes are formed at 45° relative to the Ni-O bonds, as in Fig. 1 for $\text{La}_4\text{Ni}_3\text{O}_8$. This charge ordering is accompanied by structural distortions and the opening of a gap. The Ni^{1+} atoms form an AF arrangement in analogy with the magnetism of the CuO_2 planes of the cuprate superconductors. Here we will investigate AF correlations associated with this geometry. Other layered nickelate materials^{24–27} have also been investigated with quantum simulations, especially within the classical spin-fermion method²⁸.

II. STRONG COUPLING (HEISENBERG) LIMIT

We first consider the case of localized spin-1/2 moments on the 1/3 depleted lattice with Hamiltonian

$$H = J \left[\sum_{\langle ij \rangle} \vec{S}_i \cdot \vec{S}_j + g \sum_{\langle\langle ij \rangle\rangle} \vec{S}_i \cdot \vec{S}_j \right] \quad (1)$$

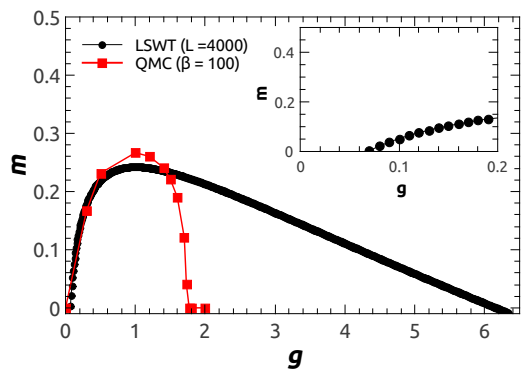


FIG. 3. Extrapolated values of the SSE results for the AF order parameter from Fig. 2 and the results of LSWT analysis, Eq. 5. With LSWT(SSE), LRAFO disappears above $g_c = 6.20 \pm 0.02$ (1.75 ± 0.01).

with exchange constants J and gJ on the two types of bonds of Fig. 1.

This model can be treated within linear spin wave theory (LSWT) by replacing the spin operators by bosonic ones via the Holstein-Primakoff (HP) transformation, and then invoking the linear approximation describing small fluctuations around the broken symmetry phase. The resulting noninteracting Hamiltonian can be diagonalized in momentum space and through a Bogliubov rotation. The spin wave spectrum is,

$$\omega(J^*, k) = J^* \sqrt{1 - \frac{|\gamma(\vec{k})|^2}{J^{*2}}}, \quad (2)$$

where,

$$\begin{aligned} \gamma(\vec{k}) &= \sum_{\delta} J(\delta) e^{-i\vec{k} \cdot \vec{r}_{\delta}} \\ &= J \left[e^{-i((\vec{k} \cdot \vec{a}_1) + (\vec{k} \cdot \vec{a}_2))/3} + e^{i((\vec{k} \cdot \vec{a}_1) - 2(\vec{k} \cdot \vec{a}_2))/3} \right] \\ &\quad + gJ e^{i(2(\vec{k} \cdot \vec{a}_1) - (\vec{k} \cdot \vec{a}_2))/3} \end{aligned} \quad (3)$$

with lattice vectors $\vec{a}_1 = 2\hat{x} - \hat{y}$ and $\vec{a}_2 = \hat{x} + \hat{y}$. Here $J^* = \sum_{\delta} J(\delta)$ is the sum of exchange constants over near neighbor sites. The AFM staggered order parameter,

$$m_s = \frac{1}{N} \left(\sum_{i \in A} \langle S_i^z \rangle - \sum_{i \in B} \langle S_i^z \rangle \right). \quad (4)$$

is obtained in the LSWT, writing $\langle S_i^z \rangle$ in terms of HP operators. At $T = 0$, we obtain:

$$m_s = S + \frac{1}{2} - \frac{1}{N} \sum_{\vec{k}} \left(1 - \frac{|\gamma(\vec{k})|^2}{J^{*2}} \right), \quad (5)$$

where S is the spin.

We can also treat the Hamiltonian more exactly on lattices of finite size using the stochastic series expansion (SSE) quantum Monte Carlo method^{29,30}. SSE samples terms in the power expansion of $e^{-\beta\hat{H}}$ in the partition function. Operator loop (cluster) updates perform the sampling efficiently²⁹. The square of the staggered magnetization, $\langle m_s^2 \rangle$, can be evaluated to high precision, and extrapolated to the thermodynamic limit.

Figure 2 shows the results of SSE simulations for different values of the bond anisotropy g and inverse linear system size $1/L$. The order parameter first increases with g , reaching a maximum at the honeycomb limit $g = 1$, and finally begins to decrease. LRAFO vanishes above $g_c = 1.75 \pm 0.01$. The extrapolated order parameter from SSE (Fig. 2) and from LSWT (Eq. 5) is given in Fig. 3. LSWT greatly overestimates the persistence of LRAFO at large g . It also predicts a quantum phase transition at small, but nonzero, $g_c = 0.065 \pm 0.005$. Similar to the case of a square lattice with anisotropic exchange^{31–33}, a zero g_c is expected here though a small nonzero value is obtained in our calculations due to finite size effect.

We emphasize the contrast of these results with those of the Heisenberg model on 1/5-depleted lattice¹² appropriate to modeling CaV_4O_9 where the lower $g_c = 0.60 \pm 0.05$. The difference, as for the case of the anisotropic square lattice, is that for the 1/5 depleted case the building blocks are small clusters (either dimers or four site plaquettes) in both the g small and g large limits. In the present case, two site clusters are formed for large g , but the small g limit still has extended 1-d structures. These give rise to LRAFO even for small g .

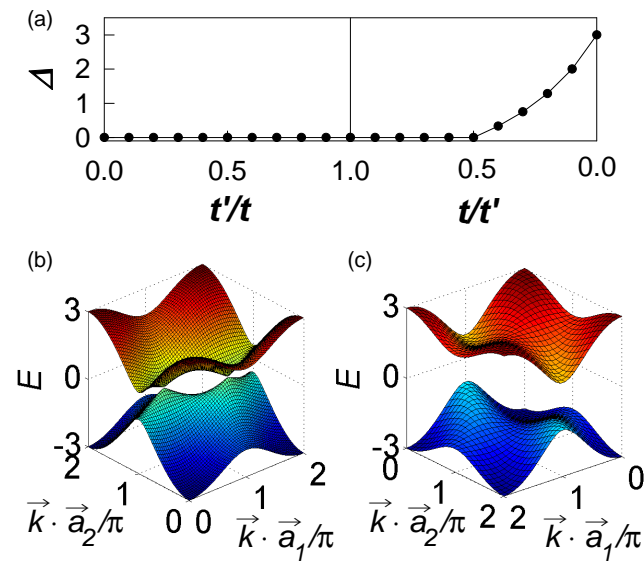


FIG. 4. (a) Band gap Δ as a function of the ratio of hopping. Δ vanishes for $t'/t < 2$. The noninteracting limit is a band insulator ($\Delta > 0$) for $t'/t > 2$. (b) Semi-metallic band structure at $t'/t = 0.5$. (c) Insulating band structure at $t'/t = 0.25$.

III. ITINERANT LIMIT

We next consider itinerant electrons, a single band Hubbard Hamiltonian on the same 1/3-depleted lattice,

$$H = -t \sum_{\langle ij \rangle \sigma} (c_{i\sigma}^\dagger c_{j\sigma} + c_{j\sigma}^\dagger c_{i\sigma}) - t' \sum_{\langle\langle ij \rangle\rangle \sigma} (c_{i\sigma}^\dagger c_{j\sigma} + c_{j\sigma}^\dagger c_{i\sigma}) + U \sum_i (n_{i\uparrow} - \frac{1}{2})(n_{i\downarrow} - \frac{1}{2}) \quad (6)$$

The hoppings along and between the one dimensional chains are t and t' , respectively. The properties of this model are solved using the determinant QMC method³⁴. In this method the partition function is expressed as a path integral. The discretization of inverse temperature β enables the isolation of the quartic interaction terms which are decoupled via a Hubbard-Stratonovich (HS) transformation. The resulting quadratic fermionic trace is done analytically, and the HS field is then sampled stochastically. Because the scaling is cubic in the lattice size N we study systems only up to $N = 2 \times 12 \times 12$ sites in contrast to the spin models described in the previous section where SSE scales linearly in N and systems up to $N = 1600$ (or more) are accessible. Equation (6) is written in particle-hole symmetric form so that the lattice is half-filled $\rho = \langle n_{i\uparrow} + n_{i\downarrow} \rangle = 1$ for all lattice sites i and any values of t', U and temperature T . At this electron density, simulations are possible down to low T without encountering the fermion sign problem³⁵.

In the noninteracting limit of Eq. (6) we have two bands with dispersion,

$$E(\vec{k}) = \pm \left[(t + t \cos(\vec{k} \cdot \vec{a}_2) + t' \cos(\vec{k} \cdot \vec{a}_1))^2 + (t \sin(\vec{k} \cdot \vec{a}_2) + t' \sin(\vec{k} \cdot \vec{a}_1))^2 \right]^{1/2} \quad (7)$$

Here the noninteracting band width w is kept fixed, $w = 4t + 2t' = 6$, as t'/t varies, setting the the energy scale $w = 6$ throughout the paper. As illustrated in Fig. 4(a), the band gap Δ vanishes for $t'/t < 2$. These bands touch at two Dirac points for $t'/t = \frac{1}{2}$ in Fig. 4(b). Figure 4(c) shows the band insulating case, $t'/t = 0.25$.

To characterize the magnetic properties of Eq. 6 we measure the AF structure factor

$$S_{\text{AF}} = \frac{1}{N} \sum_{l,j} (-1)^l \langle \vec{S}_j \cdot \vec{S}_{l+j} \rangle \quad (8)$$

where the factor $(-1)^l = +1(-1)$ if site l is on the same(different) sublattice of the bipartite structure of Fig. 1.

The spin correlation in the singlet phase falls off exponentially with separation l and S_{AF} is independent of lattice size. If LRAFO is present, $S_{\text{AF}} \propto N$, since

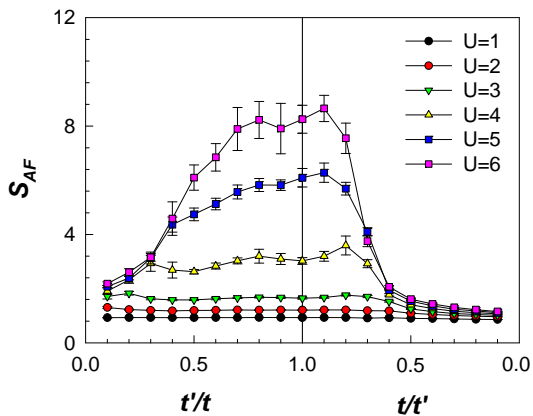


FIG. 5. The AF structure factor S_{AF} is shown as a function of hopping anisotropy for different U . The linear lattice size $L = 8$ so that the number of sites $N = 128$. (There are 64 unit cells each with two sites). The inverse temperature discretization $\Delta\tau = \beta/L = 1/2U$ except for $U = 1$ where $\Delta\tau = 1/4$. Data were acquired from 25 simulations of 1000 equilibration and 4000 measurement sweeps for each t'/t .

spin correlations remain nonzero out to all distances on a finite lattice.

Figure 5 shows S_{AF} on an $N = 8 \times 8$ lattice for different U as a function of t'/t . It is known that LRAFO exists at the symmetric honeycomb lattice point $t = t'$ only when U is sufficiently large^{36–39}, with the most accurate value⁴⁰ of the critical point $U_c = 3.869 \pm 0.013$. The data of Fig. 5 is suggestive of this result, with S_{AF} being essentially independent of the value of t'/t for $U = 1, 2, 3$, and becoming both larger and sensitive to the anisotropy for $U \geq 4$.

Finite size scaling can be used to analyze quantitatively the possibility of LRAFO. Such data are shown in Fig. 6. We find that hopping anisotropy increases U_c , in agreement with our results for the g dependence of the order parameter in the strong coupling Heisenberg model (Fig. 3) which falls off to either side of $g = 1$.

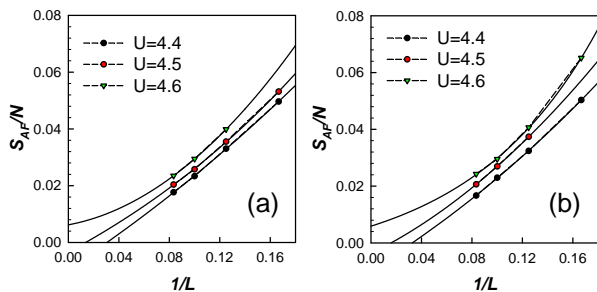


FIG. 6. Finite size scaling of the AF structure factor S_{AF} for $t'/t = 0.95$ (a) and $t'/t = 0.90$ (b). In both cases $U_c > 4.5$ is well above the critical interaction strength $U_c = 3.869$ for isotropic hopping⁴⁰.

A second diagnostic of magnetic order is the near-neighbor spin correlation between adjacent pairs of

sites. This can be evaluated for both intra- and inter-chain bonds, and measures the formation of singlet correlations, m_t and $m_{t'}$ respectively, on the associated bonds. Fig. 7 shows m_t and $m_{t'}$ for different values of U . For the Heisenberg limit, $U \rightarrow \infty$, we use $J \sim t^2/U$ to convert $g = J'/J$ to $\sqrt{t'/t}$. In the strong coupling limit $\langle S_i \cdot S_j \rangle = -3/4$ for a singlet. Here in the Hubbard model, the finite value of the on-site repulsion, $U < \infty$, allows for charge fluctuations which reduce the magnitude of the singlet correlator. The quantities m_t and $m_{t'}$ have opposite trends in the two regimes $t' < t$ and $t < t'$ of Fig. 7. When $t'/t < 1$, m_t is suppressed, and $m_{t'}$ increases and saturates with decreasing t'/t . This supports the physical scenario in which singlets are formed between the stronger t' bonds. On the other hand, if $t'/t < 1$, $m_{t'}$ is diminished. m_t approaches the short range AF correlations of the 1-d chains⁴¹, without the formation of singlets on the t bonds. Thus although at first glance Fig. 5 indicates similar, reduced values for S_{AF} for both small t'/t and for small t/t' , the singlet correlator of Fig. 7 suggests these are rather distinct limits: full singlets form at $t'/t \rightarrow 0$ but not $t/t' \rightarrow 0$.

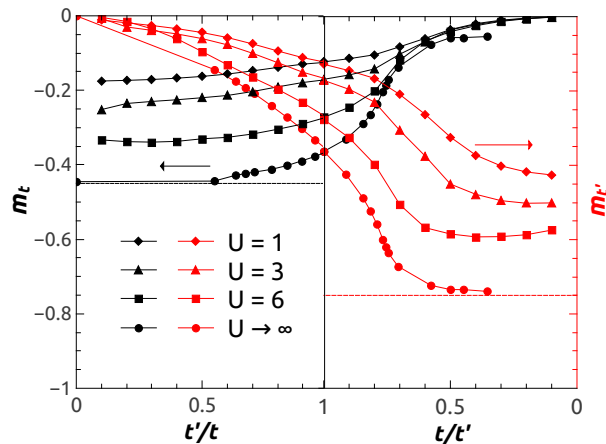


FIG. 7. Near neighbor (singlet) spin correlation function across intra- and inter-chain bonds, m_t and $m_{t'}$, respectively. $\langle S_i \cdot S_j \rangle$ is large and independent of t'/t for $t'/t \gtrsim 2$. This value matches the point at which a nonzero gap Δ opens in the spectrum, Fig. 4(a). The limiting value at $t' = 0$ ($t = 0$) is 0.4515 ⁴¹ (0.75).

The evaluation of these magnetic correlations allows us to sketch the phase diagram in the plane of hopping anisotropy and interaction strength shown in Fig. 8. The fact that $g_c = 1.75$ in the Heisenberg limit is less than the anisotropy required to open a nonzero gap Δ in the non-interacting band structure suggests that the destruction of LRAFO involves more than the simple RPA-like criterion of the vanishing of the density of states at the Fermi level. That is, the competing possibility of singlet formation also plays a role in the absence of LRAFO.

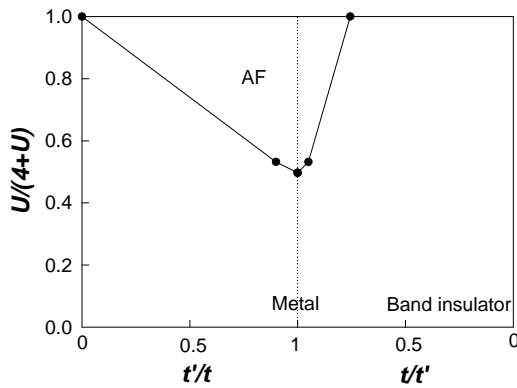


FIG. 8. Phase diagram. The $U = \infty$ Heisenberg limit is along the top of the figure, $U/(4+U) = 1$, and is extracted from the data of Fig. 3. The critical interaction strength diverges even prior to entry into the band insulator phase at $t/t' = 0.5$.

IV. CONCLUSION

In this paper we have investigated magnetic ordering on a two dimensional lattice formed by the regular removal of one third of the sites from a square lattice. We analyzed the strong coupling, Heisenberg limit using spin-wave theory and QMC (SSE), and determined the range of the ratio J'/J on the two types of bonds in which an ordered AF phase exists at $T = 0$. Unlike the one fifth depleted lattice, which breaks into small clusters in both the $J = 0$ and $J' = 0$ limits, we have shown that AF order persists to very small J'/J as a consequence of the fact that extended one dimensional chains are still present when $J' = 0$.

We also used DQMC to study the single band Hubbard Hamiltonian on this lattice. The singlet correlator was

found to grow rapidly for $t'/t \sim 1.5$, coinciding with a loss of AF order and the approach to the band insulator at $t'/t > 2$ in the noninteracting limit. The critical interaction strength $U_c \sim 3.87$ for $t = t'$ was shown to increase with inhomogeneity $t' \neq t$. The effect of *random* removal of sites on AF order has been studied in both itinerant and localized models⁴²⁻⁴⁶.

The one third depleted geometry that we investigated has recently been shown to be realized as a result of charge stripe ordering in the nickelates^{22,23}, so our simulations speak to the conditions for AF order in those materials. The relative strengths of first and second neighbor exchange couplings for nickelates has not yet been addressed. Another key feature is the presence of multiple NiO_2 layers and the surprising nature of charge equivalence between the layers^{22,23}. We cannot immediately address this phenomenon, since in our treatment charge ordering is put in *a priori* through our consideration of a one third depleted lattice and, in addition, our restriction to a single layer model.

A more approximate method than DQMC, which considers itinerant electrons interacting with classical spins^{47,48} can be employed to treat multiple bands. It may be used to explore the *spontaneous* formation of charge ordering, and we leave the details of this to future study.

V. ACKNOWLEDGEMENTS:

H.G. acknowledges support from China Scholarship Council. T.M. acknowledges funding from Science Without Borders, Brazil. The work of W.E.P. was supported by DOE grant DE-FG02-04ER46111. The work of R.T.S. was supported by DOE grant DE-SC0014671.

¹ "A Numerical Study of the Two-Dimensional Hubbard Model with Repulsive Coulomb Interaction," S.R. White, D.J. Scalapino, R.L. Sugar, E.Y. Loh, Jr., J.E. Gubernatis, and R.T. Scalettar, Phys. Rev. B40, 506 (1989).
² D.J. Scalapino, Does the Hubbard Model Have the Right Stuff? in "Proceedings of the International School of Physics", edited by R.A. Broglia and J.R. Schrieffer (North-Holland, New York, 1994), and references cited therein.
³ "Non-Perturbative Many-Body Approach to the Hubbard Model and Single-Particle Pseudogap", Y.M. Vilk and A.-M.S. Tremblay, J. Phys. I 7, 1309 (1997).
⁴ "Pairing Correlations in the Two-Dimensional Hubbard Model," S. Zhang, J. Carlson, J.E. Gubernatis, Phys. Rev. Lett. 78, 4486 (1997).
⁵ "*d*-Wave Superconductivity in the Hubbard Model", Th. Maier, M. Jarrell, Th. Pruschke, and J. Keller, Phys. Rev. Lett. 85, 1524 (2000).
⁶ "Cellular-dynamical mean-field theory of the competition between antiferromagnetism and *d*-wave superconductivity

in the two-dimensional Hubbard model", M. Capone and G. Kotliar, J. Mag. and Mag. Mat. 310, 529 (2007).
⁷ "Momentum space anisotropy and pseudogaps: a comparative cluster dynamical mean field analysis of the doping-driven metal-insulator transition in the two dimensional Hubbard model," E. Gull, M. Ferrero, O. Parcollet, A. Georges, and A.J. Millis, Phys. Rev. B82, 155101 (2007).
⁸ "Striped superconductors: how spin, charge and superconducting orders intertwine in the cuprates," E. Berg, E. Fradkin, S.A. Kivelson and J.M. Tranquada, New J. Phys. 11, 115004 (2009).
⁹ "Two Theorems on the Hubbard Model," E.H. Lieb, Phys. Rev. Lett. 62, 1201 (1989).
¹⁰ "Spin Gap in 2-Dimensional Heisenberg-Model for CaV_4O_9 ," N. Katoh and M. Imada, J. Phys. Soc. Jpn. 64, 4105 (1995).
¹¹ "Plaquette Resonating-Valence-Bond Ground State of CaV_4O_9 ," K. Ueda, H. Kontani, M. Sgrist, and P. A.Lee, Phys. Rev. Lett. 76, 1932 (1996).

- ¹² “Phase Diagram of Depleted Heisenberg Model for CaV_4O_9 ,” M. Troyer, H. Kontani, and K. Ueda, *Phys. Rev. Lett.* **76**, 3822 (1996).
- ¹³ “Convergent Expansions for Properties of the Heisenberg Model for CaV_4O_9 ,” M. P. Gelfand, Weihong Zheng, R.R.P. Singh, J. Oitmaa, and C. J. Hamer, *Phys. Rev. Lett.* **77**, 2794 (1996).
- ¹⁴ “Impact of Structure on Magnetic Coupling in CaV_4O_9 ,” W. E. Pickett, *Phys. Rev. Lett.* **79**, 1746 (1997).
- ¹⁵ “A Novel Large Moment Antiferromagnetic Order in $\text{K}_{0.8}\text{Fe}_{1.6}\text{Se}_2$ Superconductor,” B. Wei, H. Qing-Zhen, C. Gen-Fu, M. A. Green, W. Du-Ming, H. Jun-Bao, and Q. Yi-Ming, *Chin. Phys. Lett.* **28**, 086104 (2011).
- ¹⁶ “Common Crystalline and Magnetic Structure of Superconducting $\text{A}_2\text{Fe}_4\text{Se}_5$ ($\text{A}=\text{K},\text{Rb},\text{Cs},\text{Tl}$) Single Crystals Measured Using Neutron Diffraction,” F. Ye, S. Chi, W. Bao, X. F. Wang, J. J. Ying, X. H. Chen, H. D. Wang, C. H. Dong, and M. Fang, *Phys. Rev. Lett.* **107**, 137003 (2011).
- ¹⁷ “Making massless Dirac fermions from a patterned two-dimensional electron gas,” C.H. Park and S.G. Louie, *Nano Lett.* **9**, 1793 (2009).
- ¹⁸ “Designer Dirac fermions and topological phases in molecular graphene,” K.K. Gomes, W. Mar, W. Ko, F. Guinea, and H.C. Manoharan, *Nature* **483**, 306 (2012).
- ¹⁹ “Artificial honeycomb lattices for electrons, atoms and photons,” M. Polini, F. Guinea, M. Lewenstein, H.C. Manoharan, and V. Pellegrini, *Nature Nanotechnology* **8**, 625 (2013).
- ²⁰ “Electron fractionalization in two-dimensional graphene-like structures,” C.-Y. Hou, C. Chamon, and C. Mudry, *Phys. Rev. Lett.* **98**, 186809 (2007).
- ²¹ “Unconventional superconductivity on honeycomb lattice: theory of Kekulé order parameter,” B. Roy and I.F. Herbut, *Phys. Rev.* **B82**, 035429 (2010).
- ²² “Stacked charge stripes in the quasi-2D trilayer nickelate $\text{La}_4\text{Ni}_3\text{O}_8$,” J. Zhang, Y.-S. Chen, D. Phelan, H. Zheng, M.R. Norman, and J.F. Mitchell, *Proc. Nat. Acad. Sci.* **113**, 8945 (2016).
- ²³ “Charge ordering in $\text{Ni}^{1+}/\text{Ni}^{2+}$ nickelates: $\text{La}_4\text{Ni}_3\text{O}_8$,” and $\text{La}_3\text{Ni}_2\text{O}_6$,” A.S. Botana, V. Pardo, W.E. Pickett and M.R. Norman, *Phys. Rev.* **B94**, 081105(R) (2016).
- ²⁴ “Simultaneous Ordering of Holes and Spins in $\text{La}_2\text{NiO}_{4.125}$,” J.M. Tranquada, D.J. Buttrey, V. Sachan, and J.E. Lorenzo, *Phys. Rev. Lett.* **73**, 1003 (1994).
- ²⁵ “Charge and spin ordering in $\text{La}_{2-x}\text{Sr}_x\text{NiO}_{4.00}$ with $x = 0.135$ and 0.20 ,” V. Sachan, D.J. Buttrey, J.M. Tranquada, J.E. Lorenzo, and G. Shirane, *Phys. Rev.* **B51**, 12742 (1995).
- ²⁶ “Stripe order at low temperatures in $\text{La}_{2-x}\text{Sr}_x\text{NiO}_4$ with $0.289 \leq x \leq 0.5$,” H. Yoshizawa, T. Kakeshita, R. Kajimoto, T. Tanabe, T. Katsufuji, and Y. Tokura, *Phys. Rev.* **B61**, R854(R) (2000).
- ²⁷ “Spontaneous rearrangement of the checkerboard charge order to stripe order in $\text{La}_{1.5}\text{Sr}_{0.5}\text{NiO}_4$,” R. Kajimoto, K. Ishizaka, H. Yoshizawa, and Y. Tokura, *Phys. Rev.* **B67**, 014511 (2003).
- ²⁸ “Orbital Ordering, New Phases, and Stripe Formation in Doped Layered Nickelates,” T. Hotta and E. Dagotto, *Phys. Rev. Lett.* **92**, 227201 (2004).
- ²⁹ “Quantum Monte Carlo with Directed Loops”, O.F. Syljuasen and A. W. Sandvik, *Phys. Rev.* **E66**, 046701 (2002).
- ³⁰ “Order-disorder transition in a two-layer quantum antiferromagnet,” A.W. Sandvik and D.J. Scalapino, *Phys. Rev. Lett.* **72**, 2777 (1994).
- ³¹ “A plane of weakly coupled Heisenberg chains: theoretical arguments and numerical calculations,” I. Affleck, M.P. Gelfand, and R.R.P. Singh, *J. Phys. Math. Gen.* **27**, 7313 (1994).
- ³² “The Ground State of Quasi-One-Dimensional Heisenberg Antiferromagnets,” T. Sakai and M. Takahashi, *J. Phys. Soc. Japan* **58**, 3131 (1989).
- ³³ “Multichain Mean-Field Theory of Quasi-One-Dimensional Quantum Spin Systems,” A.W. Sandvik, *Phys. Rev. Lett.* **83**, 3069 (1999).
- ³⁴ “Monte Carlo calculations of coupled boson-fermion systems. I,” R. Blankenbecler, R. L. Sugar, and D. J. Scalapino, *Phys. Rev.* **D24**, 2278 (1981).
- ³⁵ “The Sign Problem in the Numerical Simulation of Many Electron Systems,” E.Y. Loh, J.E. Gubernatis, R.T. Scalettar, S.R. White, D.J. Scalapino, and R.L. Sugar, *Phys. Rev.* **B41**, 9301 (1990).
- ³⁶ “Ground-state and finite-temperature signatures of quantum phase transitions in the half-filled Hubbard model on a honeycomb lattice,” T. Paiva, R.T. Scalettar, W. Zheng, R.R.P. Singh, and J. Oitmaa, *Phys. Rev.* **B72**, 085123 (2005).
- ³⁷ “Quantum spin liquid emerging in two-dimensional correlated Dirac fermions,” Z. Meng, T. Lang, S. Wessel, F. Assaad, and A. Muramatsu, *Nature (London)* **464**, 847 (2010).
- ³⁸ “Quantum phase transitions in the Kane-Mele-Hubbard model,” M. Hohenadler, Z.Y. Meng, T.C. Lang, S. Wessel, A. Muramatsu, and F.F. Assaad, *Phys. Rev.* **B85**, 115132 (2012).
- ³⁹ “Particle-hole symmetry and interaction effects in the Kane-Mele-Hubbard model,” D. Zheng, G.-M. Zhang, and C. Wu, *Phys. Rev.* **B84**, 205121 (2011).
- ⁴⁰ “Absence of a Spin Liquid Phase in the Hubbard Model on the Honeycomb Lattice,” S. Sorella, Y. Otsuka, and S. Yunoki, *Sci. Rep.* **2**, 992 (2012).
- ⁴¹ “Linear magnetic chains with anisotropic coupling,” J.C. Bonner and M.E. Fisher, *Phys. Rev.* **135**, A640 (1964).
- ⁴² “Disorder and Impurities in Hubbard Antiferromagnets”, M. Ulmke, P. J. H. Denteneer, V. Janis, R. T. Scalettar, A. Singh, D. Vollhardt, and G. T. Zimanyi, *Adv. Sol. St. Phys.* **38**, 369 (1999).
- ⁴³ “Impurity effects at finite temperature in the two-dimensional $S = 1/2$ Heisenberg antiferromagnet,” K.H. Hoglund and A.W. Sandvik, *Phys. Rev.* **B70**, 024406 (2004).
- ⁴⁴ “Low-Temperature Properties of the Randomly Depleted Heisenberg Ladder”, M. Sigrist and A. Furusaki, *J. Phys. Soc. Jpn.* **65**, 2385 (1996)
- ⁴⁵ “Order by Disorder from Nonmagnetic Impurities in a Two-Dimensional Quantum Spin Liquid”, S. Wessel, B. Normand, M. Sigrist, and S. Haas, *Phys. Rev. Lett.* **86**, 1086 (2001).
- ⁴⁶ “Impurity-Induced Magnetic Order in Low-Dimensional Spin-Gapped Materials”, J. Bobroff, N. Laflorencie, L. K. Alexander, A.V. Mahajan, B. Koteswararao, and P. Mendels, *Phys. Rev. Lett.* **103**, 047201 (2009).
- ⁴⁷ “Colossal magnetoresistance observed in Monte Carlo simulations of the one- and two-orbital models for manganites,” C. Sen, G. Alvarez, H. Aliaga, and E. Dagotto, *Phys. Rev.* **B73**, 224441 (2006).

- ⁴⁸ First Order Colossal Magnetoresistance Transitions in the Two-Orbital Model for Manganites^{*}, C. Sen, G. Alvarez, and E. Dagotto, Phys. Rev. Lett. 105, 097203 (2010).